

MZR Resonators Etched in Microstrip Patch with Enhanced Bandwidth and Reduced Size

Xiao-Feng Li¹, Lin Peng^{1, 2, *}, Jing Ma³, Bin Shi³, Xiao-Ming Li¹, and Xing Jiang¹

Abstract—Two mu-zero resonance (MZR) resonators are etched in the patch of a microstrip antenna. The two MZR resonators generate two new resonances. As the MZR resonances are lower than the microstrip antenna resonance and the resonances merge with each other, size reduction and bandwidth enhancement were obtained. A prototype was designed and measured. The measured impedance bandwidth increased from 640 MHz (5.31–5.95 GHz, 11.33%) of the referenced microstrip antenna (RMA) to 940 MHz (4.99–5.93 GHz, 17.22%) of the proposed MZR loaded microstrip antenna (MZR-MA). Moreover, the patch size is decreased from $0.354\lambda_l \times 0.283\lambda_l$ of the RMA to $0.332\lambda_l \times 0.266\lambda_l$ of the MZR-MA, and unidirectional radiation patterns are obtained for the microstrip patch and MZR resonances. A microstrip line based model was built to analyze the MZR resonators.

1. INTRODUCTION

The zeroth-order resonator (ZOR) is attributed to metamaterials. It is very attractive in antenna design due to its extraordinary characteristics, such as very compact size from the infinite wavelength property [1, 2]. There are two kinds of ZORs, the epsilon-zero resonance (EZR) resonator with vertical polarization and the mu-zero resonance (MZR) resonator with horizontal polarization [3, 4]. However, there are common drawbacks for the ZOR antennas, such as very narrow band and small gain [1–5]. Therefore, a lot of researches were conducted to conquer these shortcomings [6–9]. In [6], a bisected structure achieved a bandwidth of 6.1% and peak gain of 1.4 dBi. In [7], the bandwidth and gain of the electromagnetic bandgap (EBG) loaded ZOR antenna were 54.2% and -2.12 dBi, respectively. In [8], the ZOR and first-order resonance were utilized to obtain an impedance bandwidth of 70.5% and antenna gains from 1.27 to 2.83 dBi. The interdigital capacitor and meander line short-circuited based ZOR antenna in [9] achieved a bandwidth of 15.1% and peak gain of 1.62 dBi. Though the above bandwidth enhanced researches present wide impedance bandwidth, the antennas have planar monopole-like structures and omnidirectional patterns. Therefore, the antennas are not suitable for unidirectional applications. In [10], complementary metamaterials with elements array were loaded in a patch antenna to adjust the higher mode frequency and convert the radiation to be broadside. Good results were obtained in [10]; however, its structure was complicated, and it was difficult to have high design efficiency.

On the other hand, microstrip antennas with broad bandwidths are highly desired. The E-shaped patches in [11] and [12] obtained bandwidths of 30.3% and 24%, respectively. The antenna sizes for [11] and [12] were $0.446\lambda_l \times 0.318\lambda_l$ and $0.504\lambda_l \times 0.313\lambda_l$, respectively, where λ_l is the free space wavelength of the lower edge frequencies. However, thick substrate is needed to lower the quality (Q) factor and to inspire the second mode for bandwidth enhancement. In [13], a shorted patch with high-profile was fed

Received 7 November 2018, Accepted 3 December 2018, Scheduled 12 December 2018

* Corresponding author: Lin Peng (penglin528@hotmail.com).

¹ Guangxi Key Laboratory of Wireless Wideband Communication and Signal Processing, Guilin University of Electronic Technology, Guilin, Guangxi 541004, China. ² School of Physics, University of Electronic Science and Technology of China, Chengdu 610054, China. ³ Science and Technology on Special System Simulation Laboratory, Beijing Simulation Center, Beijing 100854, China.

by slots etched in the ground plane, then the Q factor was reduced, and a second mode was generated for bandwidth enhancement. The antenna in [13] obtained a bandwidth of 33.6% and a patch size of $0.333\lambda_l \times 0.167\lambda_l$. However, as the patch was shorted to the ground plane, the ground plane was vital to the antenna performances, and the antenna size was much larger than the patch size. Besides, back radiation would be increased owing to the slots in the ground plane. In [14], a parasitic patch was coplanar with an L-shaped patch for compactness and broadband characteristics, and the antenna obtained a bandwidth of 6.5% and antenna size of $0.361\lambda_l \times 0.333\lambda_l$. In [15] and [16], parasitic elements were stacked upon the driven patch, and their bandwidths were 46.9% and 7.0%, respectively, while the patch sizes for [15] and [16] were $0.522\lambda_l \times 0.522\lambda_l$ and $0.327\lambda_l \times 0.270\lambda_l$, respectively. Folded patches achieved good bandwidth enhancement, such as 98.2% in [17] and 26% in [18]. The patch sizes of [17] and [18] were $0.333\lambda_l \times 0.214\lambda_l$ and $0.582\lambda_l \times 0.372\lambda_l$, respectively. However, the radiation patterns in [17] and [18] were deteriorated, and some of them were even not a unidirectional pattern. Besides, the multi-layer structures in [15–18] led to high profile and complicated construction.

ZORs can be collaborated with a microstrip antenna for bandwidth enhancement as discussed in [19, 20]. In [19] and [20], EZR-MZR resonators combining both the EZR and MZR resonances [21] were used as a parasitic element to a microstrip antenna. The ZORs in [19] and [20] required shorting pins that would complicate the structure and fabricating process. The bandwidth was increased from 2.2% of the referenced microstrip antenna to 5.1% of the ZOR-based microstrip antenna in [19]; however, the antenna size was increased by using the parasitic ZORs, and the antenna area ratio of the proposed ZOR-based microstrip antenna to the referenced microstrip antenna was approximately 1.33. Moreover, the EZR characteristic and asymmetrical structure led to oblique radiation patterns. Besides, shorting pins are required for the proposed antenna that might increase construction complexity.

In this research, microstrip antenna is loaded by novel MZR resonators for bandwidth enhancement. The MZR characteristics ensure unidirectional patterns in the whole band. As MZR resonators are very small, they are etched in the patch of a referenced microstrip antenna (RMA). Then, the resonators are coplanar with the patch for easy fabrication, and the antenna maintains compactness characteristic. It means that the proposed antenna has an identical area to the RMA. As MZR resonators generate two more resonances, the bandwidth is increased from 640 MHz (5.31–5.95 GHz, 11.33%) of the RMA to 940 MHz (4.99–5.93 GHz, 17.22%) of the MZR loaded microstrip antenna (MZR-MA). Then, the 5.15–5.825 GHz wireless local area network (WLAN) band is covered by the antenna. Good gains of 5.12–6.61 dBi are obtained for the WLAN band. Besides, as the resonant frequencies of the MZRs are lower than the microstrip resonance, the operational band is extended to lower frequency. As the RMA and MZR-MA have identical size, the downward extended band is equivalent to size reduction. Thus, the patch size is decreased from $0.354\lambda_l \times 0.283\lambda_l$ of the RMA to $0.332\lambda_l \times 0.266\lambda_l$ of the MZR-MA, where λ_l is the free space wavelength of the lower edge frequencies of the corresponding antennas.

2. ANTENNA DESIGN

An RMA was designed first as shown in Fig. 1(a). The RMA was expected to resonate in 5-GHz band. Then, its parameters were $G_1 = G_2 = 35$ mm, $a = 20$ mm, $b = 16$ mm and $d_0 = 14$ mm. The RMA was a half-wavelength resonator antenna, and it was excited at a resonant frequency f_{r0} . Note that the used substrate for antenna design in this paper had a height 4 mm and relative permittivity $\epsilon_r = 2.2$.

As shown in Fig. 1(b), two MZR resonators are embedded in the patch of the RMA to construct the MZR-MA. The left one is denoted as MZR1 and the right one denoted as MZR2. As MZRs are very compact and etched in the patch, the antenna size of the MZR-MA is equal to the RMA. As shown in the figure, the current flowing along the strips with width s produces inductance $L_{1,2}$, while the voltage gradient between the strips and patches generates capacitance $C_{1,2}$. The patch plays as ground plane for the MZRs, and then, short-end boundaries are formed to inspire resonances [4, 21]. The two MZR resonators have different sizes and resonate at different frequencies ($f_{r1} = 1/2\pi\sqrt{L_1C_1}$ and $f_{r2} = 1/2\pi\sqrt{L_2C_2}$). The parameters of the proposed MZR-MA are $G_1 = G_2 = 35$ mm, $a = 20$ mm, $b = 16$ mm, $d_0 = 14.5$ mm, $l_1 = 7$ mm, $w_1 = 4$ mm, $d_1 = 1$ mm, $d_2 = 4$ mm, $l_2 = 6.4$ mm, $w_2 = 4$ mm, $d_3 = 1.2$ mm, $d_4 = 4.1$ mm, $s = 0.5$ mm and $g = 0.2$ mm.

Then, the proposed MZR-MA antenna is the combination of three resonators, the microstrip antenna resonator, the MZR1 and the MZR2. For simplicity, the microstrip patch can be considered as

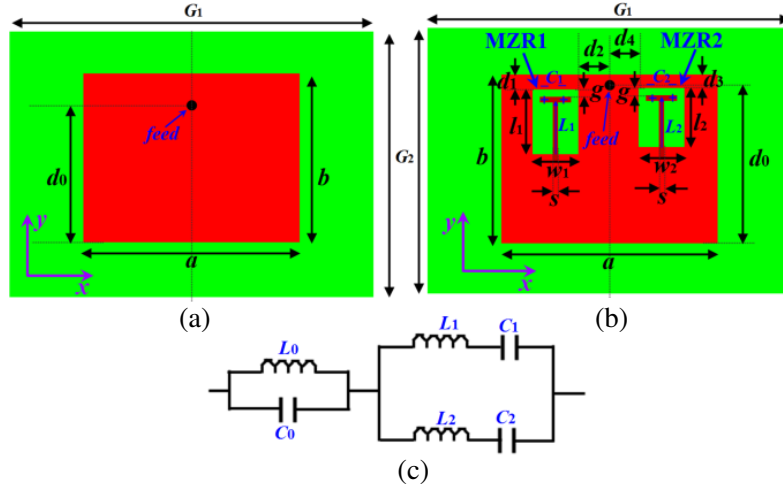


Figure 1. Schematic view of the antennas. (a) The RMA, (b) the proposed MZR-MA, and (c) equivalent circuit model of the proposed MZR-MA.

a truncated half-wavelength ($\lambda/2$) microstrip line resonator. Thus, it can be considered as a parallel LC (L_0C_0) resonator as shown in Fig. 1(c). The parallel MZR is series LC resonators (L_1C_1 and L_2C_2), and they are cascaded to the L_0C_0 as depicted in Fig. 1(c). Then, merging of the three resonators can lead to bandwidth enhancement.

To verify the MZR feature of the embedded resonators, the constitutive parameters of resonators were retrieved by a Kramers-Kronig relationship based metamaterial parameters extraction method [22]. The extraction method required scattering characteristics of the investigated object. Then, the S parameters (S_{11} , S_{21} , S_{22} and S_{12}) of the object should be calculated. For this purpose, a simple model (microstrip line based model) was built to imitate the operational environment of the MZR in the microstrip antenna as demonstrated in Fig. 2(a). As shown in Fig. 2(b), the microstrip antenna and the microstrip line have very similar current and E -field distributions. Therefore, the MZR in the microstrip antenna (patch) and in the microstrip line have similar environments. Then, the microstrip line based model could be used to investigate the MZR effect on the microstrip antenna patch. The microstrip line model used the same substrate as the designed antennas, and two ports were set at the ends of the microstrip line. The MZR is embedded in the microstrip line. Fig. 2(c) exhibits the constitutive parameter curves of the MZR1 and the MZR2. As shown in the figure, resonances occur for both the MZR1 and MZR2 as large mutations happen for the effective permittivity (ϵ_{reff}) and effective permeability (μ_{reff}) curves. The resonant frequencies for the MZR1 and the MZR2 are 5.01 GHz and 5.29 GHz, respectively. For both the MZR1 and MZR2, their ϵ_{reff} s are positive in the whole frequency band. On the other hand, their μ_{reff} s obtain small negative values almost equal to 0 at the resonances. Therefore, from the described effective LC circuit in Fig. 1(b) and the extracted constitutive parameters in Fig. 2(c), it can be judged that the embedded structures are MZR resonators.

3. RESULTS AND DISCUSSION

The curves of the Z -parameters of the RMA and MZR-MA are plotted in Fig. 3. From Z -parameters curves of the RMA, only one resonance is observed at $f_{r0} = 5.79$ GHz, while the Z -parameters curves of the MZR-MA are similar to those of the RMA except that two more peaks are observed; therefore, two extra resonances are obtained for the MZR-MA. Then, the resonances of the MZR-MA are $f_{r0} = 5.79$ GHz, $f_{r1} = 5.11$ GHz and $f_{r2} = 5.24$ GHz. The extra resonances are owing to the embedded MZR resonators, and they boost the impedances of the low frequencies, which obtain impedance matching at these frequencies. As the RMA and MZR-MA have similar Z -parameters curves (except for the MZR resonances), it is implied that the MZR resonators has little impact on the performances of a microstrip antenna.

The RMA was constructed with the measured $|S_{11}|$ shown in Fig. 4(a). The simulated $|S_{11}|$ is

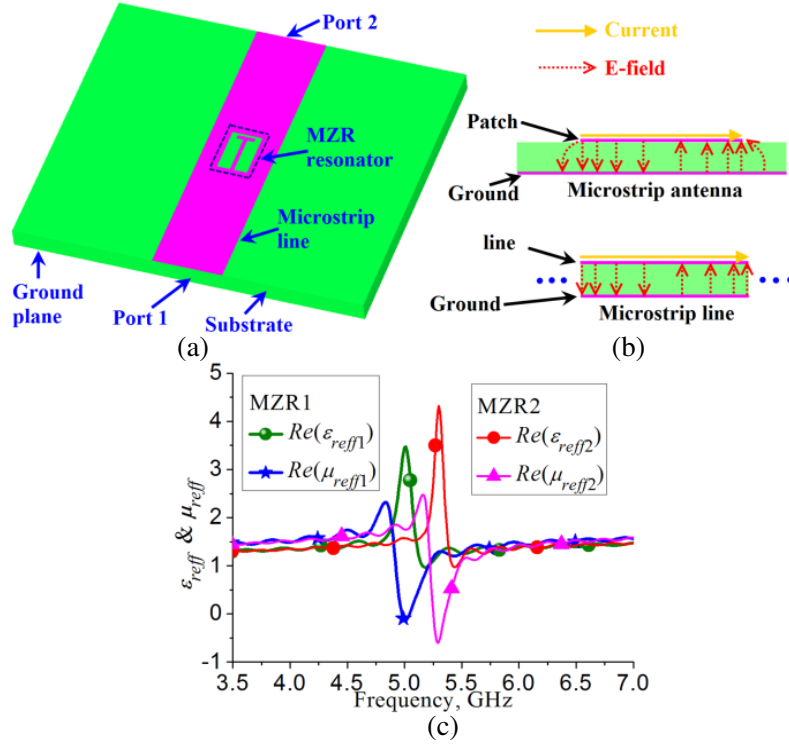


Figure 2. The constitutive parameters of the MZR resonators. (a) Simulation model, (b) currents and E -fields of the microstrip antenna and microstrip line, and (c) results.

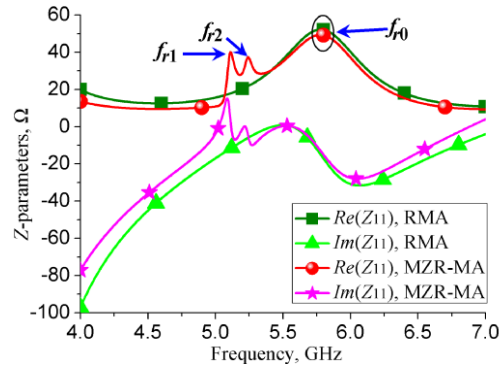


Figure 3. Z -parameters of the RMA and MZR-MA.

also plotted in Fig. 4(a) for comparison. As demonstrated in the figure, only one matching pole (f_0) is observed. The simulated and measured -10 dB bandwidths are 5.34–5.97 GHz (11.17% at $f_0 = 5.64$ GHz) and 5.31–5.95 GHz (11.33% at $f_0 = 5.65$ GHz), respectively. Good agreement is observed between the simulated and measured results. Unfortunately, 5.15–5.825 GHz WLAN band is not covered.

The proposed MZR-MA was also fabricated and measured as demonstrated in Fig. 4(b). Compared to the RMA, the simulated and measured $|S_{11}|$ results of the MZR-MA indicate two extra matching poles (f_1 and f_2) in the vicinity of the f_0 . f_1 and f_2 are inspired by the MZR1 and MZR2, respectively. Then, the enhancement of the impedance bandwidth was achieved. The simulated matching poles are $f_1 = 5.11$ GHz, $f_2 = 5.23$ GHz and $f_0 = 5.67$ GHz, and the measured matching poles are $f_1 = 5.02$ GHz, $f_2 = 5.14$ GHz and $f_0 = 5.65$ GHz. A bandwidth is defined with $|S_{11}| \leq -10$ dB. Then, the merging of the three resonances (matching poles) results in a simulated band of 5.09–5.98 GHz (16.09% at 5.53 GHz)

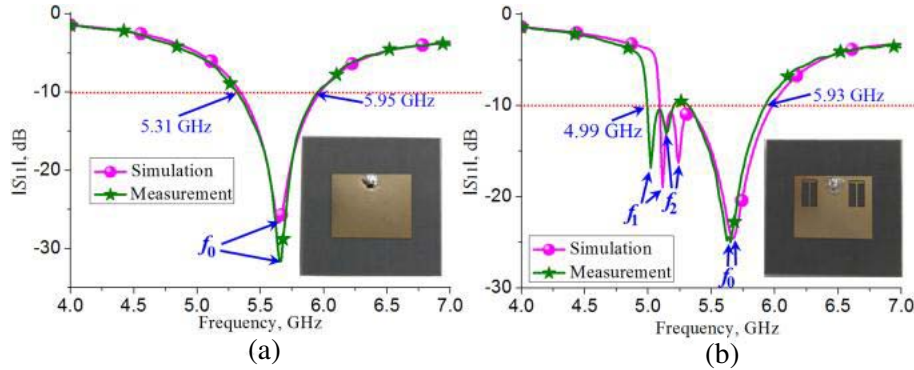


Figure 4. Simulated and measured $|S_{11}|$ of the antennas. (a) RMA, and (b) MZR-MA.

and a measured band of 4.99–5.93 GHz (17.22% at 5.46 GHz). From the following parametric studies in Fig. 6, the MZR resonances are very sensitive to the size parameters, thus, the small discrepancy observed between the simulated and measured results is probably owing to the fabrication error of the small line width and small gap of the MZRs. Both the simulated and measured bandwidths of the MZR-MA cover the 5-GHz WLAN band.

As the MZR resonators are embedded in the microstrip patch, their coupling should be considered [23]. Moreover, as the MZRs are electrically small, they are sensitive to structure parameters. Therefore, the field distributions of the resonances are presented, and the parametric studies of the MZR resonators (two parameters l_1 and l_2) are conducted. To reveal the operational mechanisms of the proposed antenna, the current and E -field distributions at the three matching poles are demonstrated in Fig. 5. Figs. 5(a), (b) and (c) plot the fields of $f_1 = 5.11$ GHz, $f_2 = 5.23$ GHz and $f_0 = 5.67$ GHz, respectively. As shown in Fig. 5(a), both the current and E -fields of $f_1 = 5.11$ GHz are concentrated on the MZR1. Therefore, f_1 is attributed to the MZR1. Besides, the currents flowing along the strip form inductance L_1 , and the E -fields focusing on the edge between the strip and the patch generate capacitance C_1 . The fields distributions of $f_2 = 5.23$ GHz shown in Fig. 5(b) are similar to that in Fig. 5(a), and they are concentrated on the MZR2. Analogously, the currents and E -fields of f_2 generate inductance L_2 and capacitance C_2 , respectively. For the fields of $f_0 = 5.67$ GHz shown in Fig. 5(c), the currents are concentrated on the right and left edges of the patch, and the E -fields are concentrated on the up and down edges of the patch. Thus, f_0 is typically a microstrip antenna resonance. Moreover, as the fields of f_0 are little distribute on the MZRs, the couplings between the resonators are small. Then, by merging the resonance of the MA with the resonances of MZRs, a wideband can be achieved.

To further reveal the advantages of the proposed antenna, two parameters (l_1 and l_2) were studied. From the current distributions of Figs. 5(a) and (b), l_1 and l_2 are related to L_1 and L_2 , respectively. Therefore, it is expected that the resonances (matching poles) of the MZR1 and MZR2 can be tuned by adjusting l_1 and l_2 , respectively. As shown in Fig. 6(a), the MZR1-related parameter l_1 is swept from 7 mm to 7.6 mm with a step of 0.3 mm. As l_1 increases from 7 mm to 7.3 mm and 7.6 mm, f_1 decreases from 5.11 GHz to 5.00 GHz and 4.77 GHz, while f_2 and f_0 are almost unchanged. As shown in Fig. 6(b), the MZR2-related parameter l_2 is swept with four parameters of 6.4 mm, 6.7 mm, 7.3 mm and 7.6 mm. It is found that the variation of l_2 has little impact on f_1 and f_0 . However, f_2 increases from 5.23 GHz to 5.37 GHz as l_2 decreases from 6.7 mm to 6.4 mm, and f_2 decreases from 5.23 GHz to 5.01 GHz and 4.90 GHz with increased from 6.7 mm to 7.3 mm and 7.6 mm. Thus, it is easy to tune the resonant frequencies independently by adjusting the resonator-related parameters.

The radiation patterns were measured in a microwave anechoic chamber with the NSI2000 system as shown in Fig. 7(a). The measured and simulated radiation patterns of f_1 , f_2 and f_0 of the MZR-MA are plotted in Figs. 7(b), (c) and (d), respectively. Owing to the restriction of the NSI2000 system, only half space was measured in this research. However, it is enough to verify the simulated results. As shown in the figure, reasonable agreements are observed between the simulations and measurements. The discrepancies between the simulation and measurement are mainly attributed to measurement errors from the fixation of the measured antenna by the self-made test fixture. Owing to the MZR features,

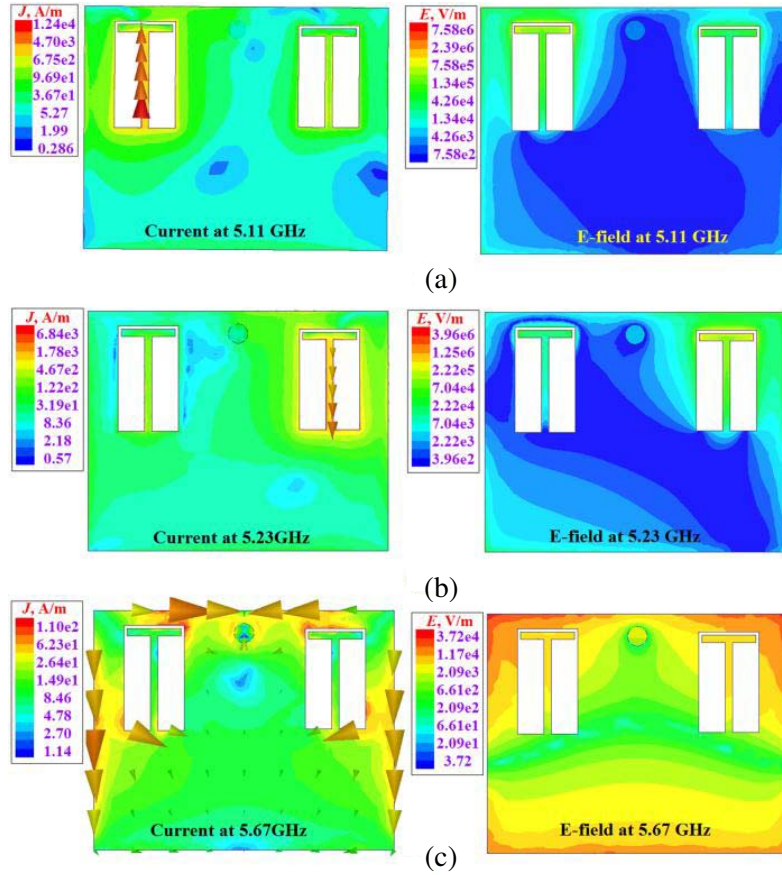


Figure 5. Current/ E -field distributions of the MZR-MA. (a) $f_1 = 5.11$ GHz, (b) $f_2 = 5.23$ GHz, and (c) $f_0 = 5.67$ GHz.

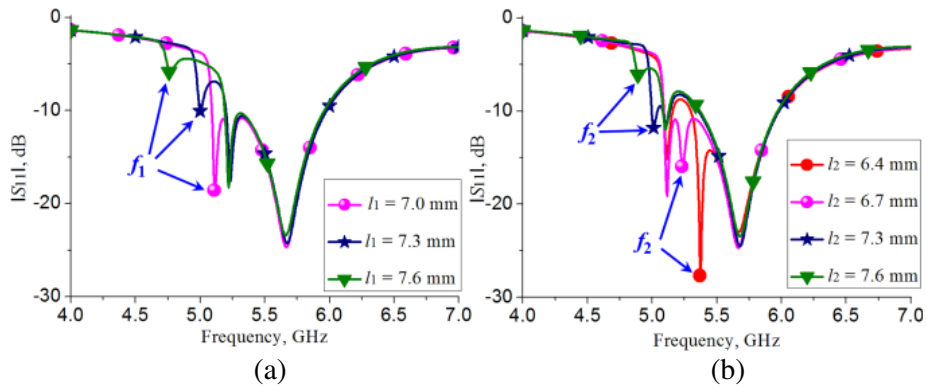


Figure 6. Parametric study. (a) l_1 , and (b) l_2 .

f_1 and f_2 demonstrate very good unidirectional patterns. Similar to normal microstrip antenna, f_0 also obtains good unidirectional patterns. It is also found that the cross-polarizations of the MZR frequencies (f_1 and f_2) are larger than that of the microstrip antenna resonant frequency (f_0). It is because the MZR disturbs the fields around them at their corresponding resonant frequencies.

The simulated/measured gains for RMA and MZR-MA are plotted in Fig. 8, and the simulated efficiencies of the antennas are also demonstrated in the figure. Reasonable agreements are observed between simulated and measured gains. For the MZR-MA, the simulated gains range from 4.85 dBi to 7.47 dBi in the 5.09–5.98 GHz band, and the measured gains range from 2.57 dBi to 6.61 dBi in the

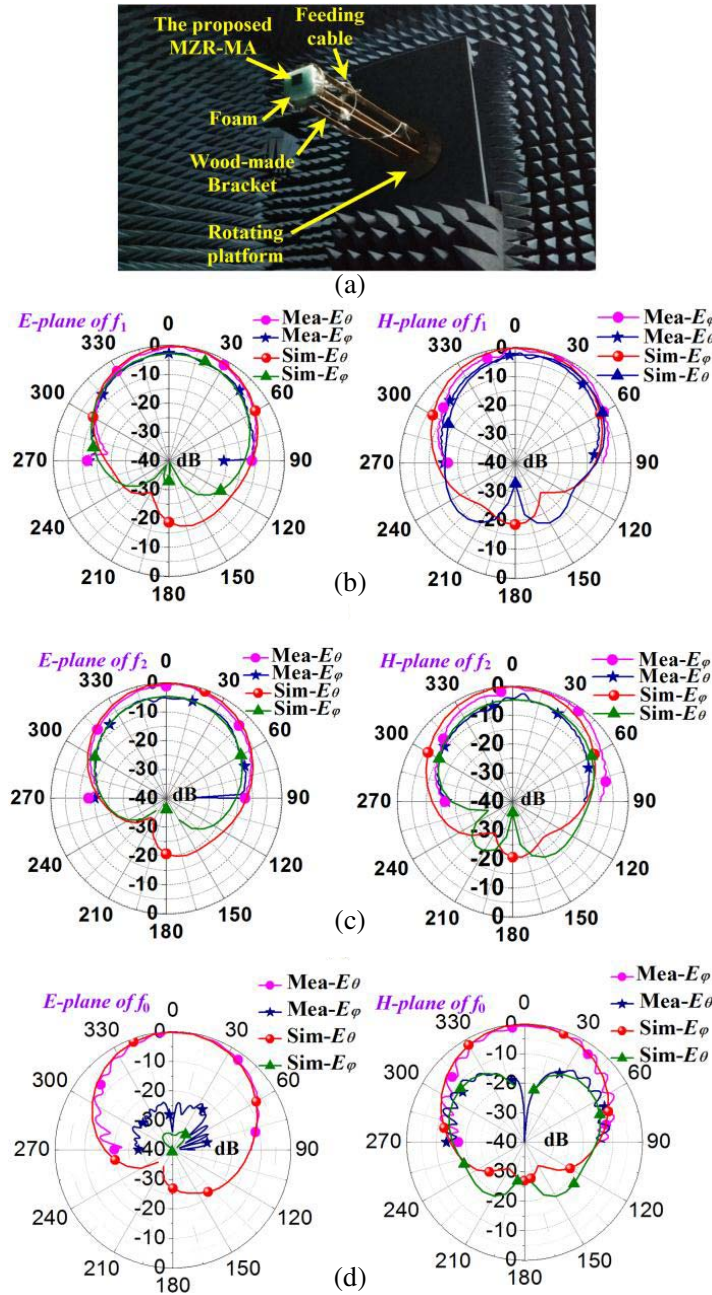


Figure 7. Radiation patterns. (a) The measuring environment, (b) f_1 , (c) f_2 , and (d) f_0 .

4.99–5.93 GHz, while the measured gains in the 5.15–5.825 GHz WLAN band range from 5.12 dBi to 6.61 dBi. As the MZR were embedded in the patch of a microstrip antenna, rather high antenna gains were obtained for the MZR resonators as compared to the reported ZOR antennas, such as [6–9]. For the RMA, the simulated gains range from 6.87 dBi to 7.53 dBi in the 5.34–5.97 GHz band, and the measured gains range from 6.22 dBi to 7.17 dBi in the 5.31–5.95 GHz band. It is also found from the figure that the MZR-MA and RMA have very similar gain characteristics in the microstrip antenna resonance band (such as the 5.3–5.9 GHz band), while the gains of the MZR resonances band (such as the 5.1–5.3 GHz band) are smaller than the microstrip antenna resonance band. As shown in Fig. 8, the RMA and MZR-MA have similar efficiencies (range from 0.85–0.95) in 5.3–5.9 GHz, while the efficiencies in the MZR resonances band (such as the 5.1–5.3 GHz band) range from 0.56 to 0.85 for the MZR-MA. As

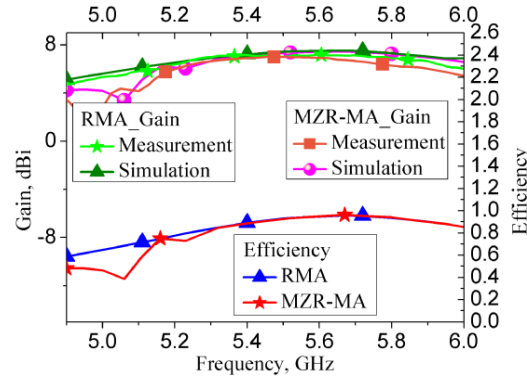


Figure 8. Gains and efficiencies of the RMA and the MZR-MA.

the size of MZR resonators are electrically small, the gains and efficiencies of the MZR resonances band are inevitably small.

4. CONCLUSION

Novel MZR resonators were used to enhance the bandwidth of a microstrip antenna to serve the 5-GHz WLAN applications. It is found that, by embedding two MZR resonators, two extra resonances were generated. By merging the new resonances with the resonance of the microstrip antenna, the bandwidth can be increased from 640 MHz of the RMA to 940 MHz of the MZR-MA. Therefore, the 5.15–5.825 GHz (675 MHz) band of the WLAN is covered. Meanwhile, the patch size is decreased from $0.354\lambda_l \times 0.283\lambda_l$ of the RMA to $0.332\lambda_l \times 0.266\lambda_l$ of the MZR-MA. Research also found that the resonances of the proposed antenna can be independently tuned by adjusting their related parameters. The proposed antenna is a good candidate for WLAN applications. The proposed designing technique by embedding ZOR (MZR) resonators in the patch of a microstrip antenna is very effective for bandwidth enhancement and size reduction of a microstrip, and it can be easily applied to other band designs.

ACKNOWLEDGMENT

This work was supported in part by the National Natural Science Foundation of China under Grant Nos. 61661011 & 61401110 & 61761012, and in part by Key Laboratory of Equipment Development Department.

REFERENCES

1. Caloz, C. and T. Itho, *Electromagnetic Metamaterials: Transmission Line Theory and Microwave Applications. (The Engineering Approach)*, Wiley & Sons, Hoboken, New Jersey, 2006.
2. Lai, A., K. M. K. H. Leong, and T. Itho, "Infinite wavelength resonant antennas with monopolar radiation pattern based on periodic structures," *IEEE Trans. Antennas Propag.*, Vol. 55, No. 3, 868–876, 2007.
3. Park, J. H., Y. H. Ryu, J. G. Lee, and J. H. Lee, "Epsilon negative zeroth-order resonator antenna," *IEEE Trans. Antennas Propag.*, Vol. 55, No. 12, 3710–3712, 2007.
4. Park, J. H., Y. H. Ryu, and J. H. Lee, "Mu-zero resonance antenna," *IEEE Trans. Antennas Propag.*, Vol. 58, No. 6, 1865–1875, 2010.
5. Lee, S. W. and J. H. Lee, "Electrically small MNG ZOR antenna with multilayered conductor," *IEEE Antennas Wireless Propag. Lett.*, Vol. 9, 724–727, 2010.
6. Yang, S. Y. and M. K. M. Ng, "A bisected miniaturized ZOR antenna with increased bandwidth and radiation efficiency," *IEEE Antennas Wireless Propag. Lett.*, Vol. 12, 159–162, 2013.

7. Sharma, S. K., A. Gupta, and R. K. Chaudhary, "Epsilon negative CPW-fed zeroth-order resonating antenna with backed ground plane for extended bandwidth and miniaturization," *IEEE Trans. Antennas Propag.*, Vol. 63, No. 11, 5197–5203, 2015.
8. Niu, B. J. and Q. Y. Feng, "Bandwidth enhancement of CPW-fed antenna based on epsilon negative zeroth- and first-order resonators," *IEEE Antennas Wireless Propag. Lett.*, Vol. 12, 1125–1128, 2013.
9. Chi, P. L. and Y. S. Shih, "Compact and bandwidth-enhanced zeroth-order resonant antenna," *IEEE Antennas Wireless Propag. Lett.*, Vol. 14, 285–288, 2015.
10. Xiong, J., X. Q. Lin, Y. F. Yu, M. Tang, and S. Xiao, "Novel flexible dual-frequency broadside radiating rectangular patch antennas based on complementary planar ENZ or MNZ metamaterials," *IEEE Trans. Antennas Propag.*, Vol. 60, No. 8, 3958–3961, 2012.
11. Yang, F., X. X. Zhang, X. N. Ye, and Y. Rahmat-Samii, "Wide-band E-shaped patch antennas for wireless communications," *IEEE Trans. Antennas Propag.*, Vol. 49, No. 7, 1094–1100, 2001.
12. Wong, K. L. and W. H. Hsu, "A broad-band rectangular patch antenna with a pair of wide slits," *IEEE Trans. Antennas Propag.*, Vol. 49, No. 9, 1345–1347, 2001.
13. Lee, K. J. and Y. S. Kim, "Broadband shorted-patch antenna with U-shaped coupling slot," *Microw. Opt. Technol. Lett.*, Vol. 53, No. 11, 2566–2569, 2011.
14. Peng, L., Y. J. Qiu, L. Y. Luo, and X. Jiang, "Bandwidth enhanced L-shaped patch antenna with parasitic element for 5.8-GHz wireless local area network applications," *Wireless Personal Communications*, Vol. 91, No. 3, 1163–1170, 2016.
15. Nasimuddin, Z. N. Chen, "Wideband microstrip antennas with sandwich substrate," *IET Microw. Antennas Propag.*, Vol. 2, No. 6, 538–546, 2008.
16. Peng, L., J. Y. Xie, X. Jiang, and S. M. Li, "Wideband microstrip antenna loaded by elliptical rings," *Journal of Electromagnetic Waves and Applications*, Vol. 30, No. 2, 154–166, 2016.
17. Malekpoor, H. and S. Jam, "Enhanced bandwidth of shorted patch antennas using folded-patch techniques," *IEEE Antennas Wireless Propag. Lett.*, Vol. 12, 198–201, 2013.
18. Guha, D., C. Sarkar, S. Dey, and C. Kumar, "Wideband high gain antenna realized from simple unloaded single patch," *IEEE Trans. Antennas Propag.*, Vol. 63, No. 10, 4562–4566, 2015.
19. Peng, L., J. M. Mao, X. F. Li, X. Jiang, and C. L. Ruan, "Bandwidth enhancement of microstrip antenna loaded by parasitic zeroth-order resonators," *Microw. Opt. Technol. Lett.*, Vol. 59, No. 5, 1096–1100, 2017.
20. Sun, K., L. Peng, Q. Li, and X. Jiang, "T/L shaped zeroth-order resonators loaded microstrip antenna with enhanced bandwidth for wireless applications," *Progress In Electromagnetics Research C*, Vol. 80, 157–166, 2018.
21. Peng, L., J. Y. Xie, X. Jiang, and C. L. Ruan, "Design and analysis of a new ZOR antenna with wide half power beam width (HPBW) characteristic," *Frequenz*, Vol. 71, No. 1–2, 41–50, 2017.
22. Szabo, Z., G. H. Park, R. Hedge, and E. P. Li, "A unique extraction of metamaterial parameters based on Kramers-Kronig relationship," *IEEE Trans. Microw. Theory Techn.*, Vol. 58, No. 10, 2646–2653, 2010.
23. Schneider, V. M. and H. T. Hattori, "High-tolerance power splitting in symmetric triple-mode evolution couplers," *IEEE J. Quantum Electron.*, Vol. 36, No. 8, 923–930, 2000.